Supporting Information

In Situ Polymerization of Polypyrrole and Polyaniline on the Surface of Magnetic Molybdenum Trioxide Nanoparticles: Implications for Water Treatment

Sofia K. Fanourakis[1‡], Sharona Q. Barroga[2,3‡], Jem Valerie D. Perez[2], Lilin He[4], and Debora F. Rodrigues[1,5*]*

[1] Department of Materials Science and Engineering, University of Houston, Houston, TX 77204 – 4003, USA

[2] Department of Chemical Engineering, University of the Philippines, 1101 Diliman, Quezon City, Philippines

[3] Department of Chemical Engineering, Mariano Marcos State University, 2906 Batac, Ilocos Norte, Philippines

[4] Neutron Scattering Division, Oak Ridge National Laboratory, Oak Ridge, Tennessee 37831-6393, USA

[5] Department of Civil and Environmental Engineering, University of Houston, Houston, TX 77204 – 4003, USA

[*]Emails: dfrigirodrigues@uh.edu; he3@ornl.gov

Experimental Design and Statistical Analysis using RSM

The Design Expert (DE) software was used to generate the total number of experiments, analyze the experimental data, and acquire the relationship between the different input parameters and output responses. The DE software estimates statistical parameters to assess the validity of the resulting models using Analysis of Variance (ANOVA).

For the synthesis of PPy@MoO_3@Fe_3O_4 (PMF1) and PPy@MoO_3@Fe_3O_4 (PMF2) sets of experiments were generated using this software. The experiments were carried out and the output responses for each respective experiment was added to the software. Models were generated by the software using reduced quadratic type modeling. Statistical significance was ensured for each term in each model using an α of 0.05 and by ensuring the lack of fit was insignificant. Furthermore, we ensured that the resulting F-values were greater than 25 for each model indicating that the signal to noise ratio was high enough to allow us to use the resulting models to predict our optimum material. Equations 1-6 describe the resulting models for each of the material and output responses as second-order equations for methylene blue (MB) dye removal and dissolution in terms of coded factors.

$$\text{PMF1 \% MB Dye Removal (Dark)} = 60.46 - 0.0642A + 5.10B - 10.09C + 9.67AB - 10.40A^2 - 21.92B^2 \quad (1)$$

$$\text{PMF1 \% MB Dye Removal (Light)} = 81.25 + 3.75A + 2.80B - 11.81C + 16.63AB + 5.68BC - 16.92A^2 - 14.33B^2 + 7.37C^2 \quad (2)$$

$$\text{PMF1 \% Dissolution} = 11.48 - 1.23A - 1.10B - 1.26C - 8.52AC - 5.45B^2 \quad (3)$$

$$\text{PMF2 \% MB Dye Removal } (Dark) = 75.72 + 2.59A - 48.4D + 4.11AD + 16.52A^2 - 71.68D^2 + 52.87A^2D \quad (4)$$

$$\text{PMF2 \% MB Dye Removal (Light)} = 81.46 + 5.36A - 100.80D + 5.60AD + 64.48A^2 - 122.14D^2 + 107.57A^2D \quad (5)$$

$$\text{PMF2 \% Dissolution} = 9.86 + 4.62A + 4.38D + 4.44AD - 5.36A^2 \quad (6)$$

where A is the amount of ammonium molybdate tetrahydrate (AMT), B is the amount of Fe_3O_4, C is the volume of pyrrole monomer, D is the amount of MoO_3@Fe_3O_4 (MF), AB is the interaction between the amount of AMT and amount of Fe_3O_4, AC is the interaction between the amount of AMT and volume of pyrrole monomer, BC is the interaction between the amount of Fe_3O_4 and volume of pyrrole monomer, AD, is the interaction between the amount of AMT in MF and the amount of MF in PMF2, and A^2, B^2, and C^2 are the quadratic terms for each of the main factors, respectively. The equation in terms of coded factors can be used to make predictions about the response for given levels of each factor. The negative sign indicates the antagonistic effects whereas the positive sign indicates the synergistic effects.[1] The obtained R_2 values shown in Table S1 for R_1, R_2 and R_3 were high (greater than 0.8) meaning that the models generated for each system have good predictability. Adequate precision of all responses was greater than 10.27 indicating adequate signals. The low standard deviations of the models for MB dye removal and dissolution also confirm the goodness of fit.

Table S1. Fit Statistics of the Responses on the Reduced Quadratic Model

	R_1: % MB Dye Removal (Dark)		R_2: % MB Dye Removal (Light)		R_3: % Dissolution	
	PMF1	PMF2	PMF1	PMF2	PMF1	PMF2
Std. Dev.	6.73	0.5796	3.04	0.4458	3.21	1.28
Mean	45.25	40.39	70.01	45.96	8.92	5.61
C.V. %	14.88	1.44	4.34	0.97	35.94	22.8
R^2	0.8981	0.9997	0.9850	0.9998	0.7994	0.9714
Adjusted R^2	0.8370	0.9994	0.9997	0.9997	0.7082	0.9599
Predicted R^2	0.6474	0.9989	0.8705	0.9993	0.5309	0.955
Adequate Precision	10.9146	153.5627	25.5967	210.6617	10.2713	24.5496

The MB dye removal efficiency and dissolution of catalyst in the solution as predicted by Equation 1 to Equation 6. The results show a good correlation between the actual values and the predicted responses. Response surface contour plots for all responses are shown in Figure S-1 and Figure S2 for PMF1 and PMF2, respectively. These plots allow us to understand the relationships of the independent variables to their responses. To understand the responses for PMF1, one of the independent variables (i.e pyrrole) was held constant at its center level to show the interaction of the remaining factors (i.e. Fe_3O_4 and MoO_3 precursor) towards the response. Figures S1a.i and S1b.i illustrate the surface of MoO_3 and Fe_3O_4 with a maximum response on MB dye removal. An increase in the amount on both factors showed an increase of MB dye removal first followed by a decrease. This trend agrees with Equation 1 and Equation 2, where the quadratic term A^2 and B^2 had a negative value indicating a downward curvature. The effects of pyrrole and MoO_3 concentrations (Figure S1.a.ii and Figure S1.b.ii) and the effects of pyrrole and Fe_3O_4 concentration (Figure S1.a.iii and 1b.iii) show a slight decrease of MB dye removal when pyrrole concentration increased. The slight upward curvature on the pyrrole was a result of the positive quadratic term (C^2) in Equation 2.

The interaction of the factors in Figure S1.c.i and 1.c.iii illustrate that there is no significant effect on the dissolution of the nanomaterials. However, the interaction of the MoO_3 and pyrrole on the dissolution of the nanomaterial as shown in Figure S1.c.ii was significant with a positive effect. The response surface contour plot illustrates a minimax response. The graph illustrates that increasing either factor while decreasing the other leads to an increase in the dissolution of the nanomaterial. Also, increasing or decreasing both factors at the same time leads to a decrease in the dissolution response.

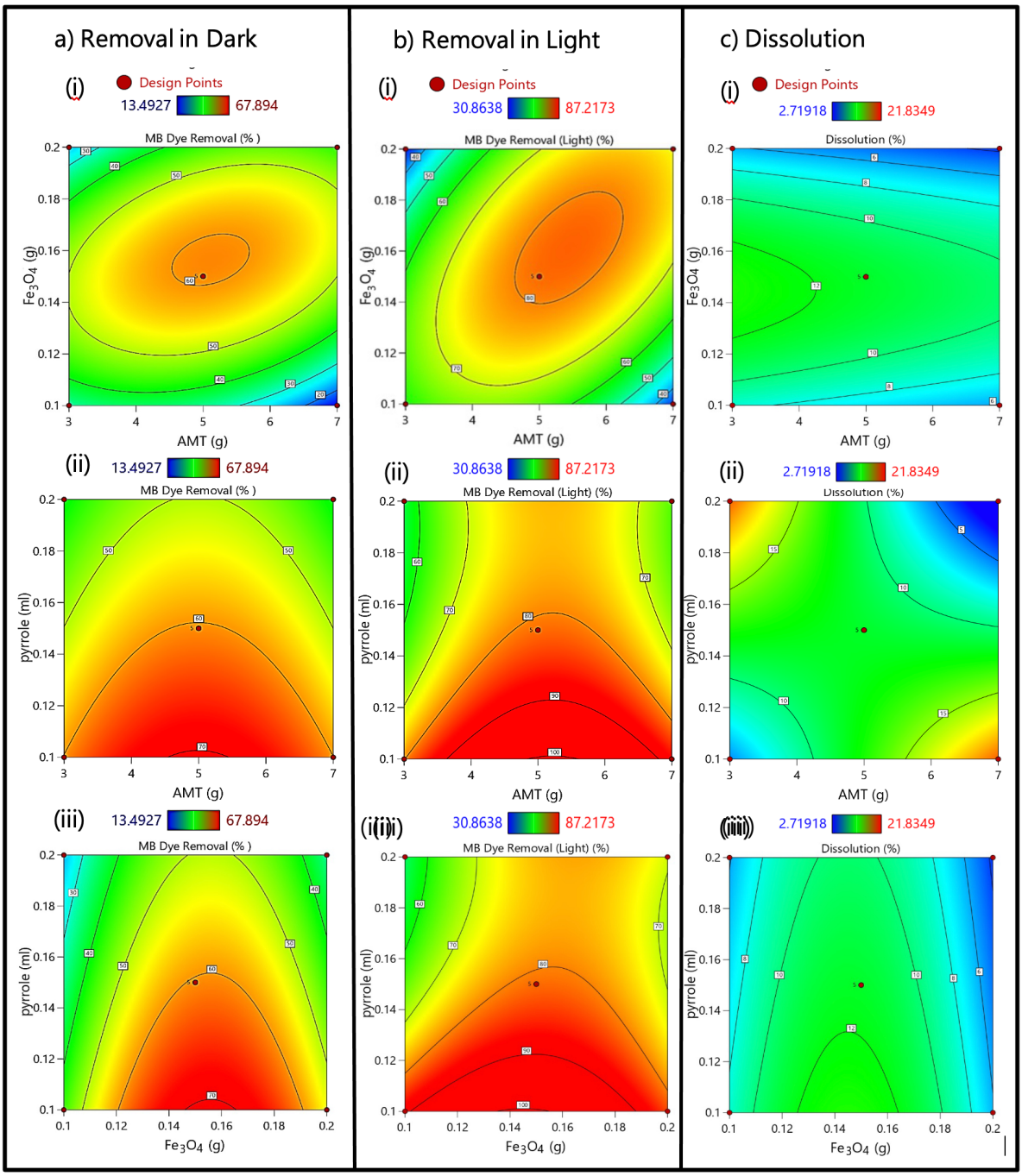

Figure S1: Contour plots of methylene blue dye removal by PMF1 in a) dark and b) light, and c) dissolution of PMF1 material where (i) amount of Fe_3O_4 vs amount of AMT (ii) volume of pyrrole vs the amount of AMT, and (iii) volume of pyrrole vs the amount of Fe_3O_4

Figure S2 shows the contour plots describing Equations (4) to (6). The MB removal in light and dark (Figure S2.a and Figure S2.b, respectively), show similar trends. The amount of MF in PMF seems to be the predominant factor as to the extent of MB removal. While the amount of

AMT results in an overall positive effect on the removal of MB (see Equations (4) and (5)), the amount of MF produced a negative effect, which was counteracted by the interaction of the amount of AMT and amount of MF in PMF. From the contour plots we can see that there was an optimum region defined for the removal of MB in the light and dark. The amount of AMT, however, was the factor that most influenced the dissolution of the material as shown in Figure S2.c This as we expected since the larger the amount of AMT was, the more molybdenum was available in the material, which could readily dissolve. However, the PANI coating could help counteract the dissolution of MoO_3 when it could coat a sufficient amount of the material.

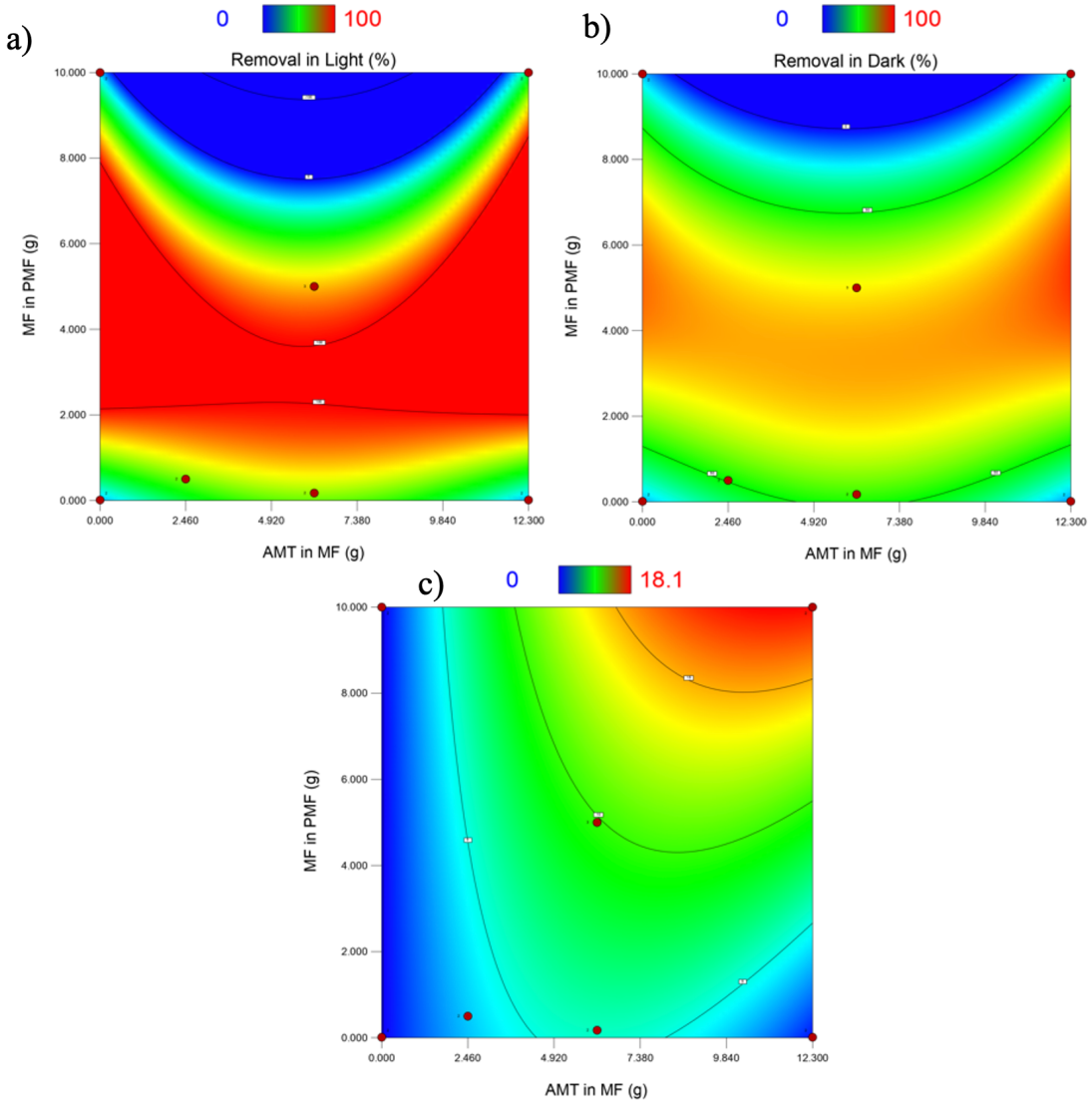

Figure S2. Contour plots of methylene blue dye removal by PMF2 in a) light, b) dark, and c) dissolution of PMF2 material

Table S2. Model Validation of the PPy@MoO_3@Fe_3O_4 (PMF1) and PANI@MoO_3@Fe_3O_4 (PMF2) synthesis from numerical optimization

Response	Nanomaterial	Predicted Mean (%)	Standard Deviation (%)	95% PI low[(a)] (%)	Data Mean (Observed) (%)	95% PI high[(a)] (%)
MB Dye Removal (Dark)	PMF1	66.12	6.73	55.21	70.26	77.02
	PMF2	59.92	0.58	57.60	60.18	62.23
MB Dye Removal (Light)	PMF1	90.75	3.04	85.65	95.39	95.85
	PMF2	75.94	0.45	74.17	75.98	77.72
Dissolution	PMF1	13.17	3.21	7.38	4.12	18.97
	PMF2	3.78	3.21	1.50	5.6	6.07

[a)]Confidence = 95%

Table S3. Comparison of our developed material with other photocatalysts in the removal of methylene blue (MB)

Material	Material and Contaminant Concentrations	Light Source	Percent Removal	Time to Achieve Removal	Ref
Bi_2O_3/MoO_3	500 ppm photocatalyst in 10 ppm MB solution	Visible, 500W	86.6%	120 min	[2]
h- MoO_3	25 ppm catalyst in 10 ppm MB solution	Visible, 350W	19 %	105 min	[3]
AgNPs decorated microstructure ZnO	600 ppm catalyst in 10 ppm MB solution	UV, 6W	87.74%	60 min	[4]
TiO_2/GO	1000 ppm catalyst in 0.01mM MB solution	Visible, 450W	51.3%	60 min	[5]
MoO_3/P25	100 ppm catalyst in 15 ppm MB solution	Visible, 110W	38%	150 min	[6]
PPy@MoO_3 @Fe_3O_4 (PMF1)	500 ppm catalyst in 40 ppm MB solution	Visible, 4W	95.39%	120 min	(this work)
PANI@MoO_3 @Fe_3O_4 (PMF2)	500 ppm catalyst in 40 ppm MB solution	Visible, 4W	75.98%	120 min	(this work)

Table S4. Material structural parameters calculated from the XRD data

Material	Crystallite size[1] (nm)	[1]Lattice strain (%)	Microstrain,[2] ε ($x10^{-3}$)	Dislocation density,[2] δ ($x10^{14}$ m^{-2})
MF1	26	0.67	1.56	21.3
PMF1	32	0.55	1.26	13.8
MF2	37	0.46	1.06	9.7
PMF2	44	0.36	0.89	6.6

[1] Calculated using Scherrer calculator form X'Pert HighScore Plus software

[2] Calculated based from the formulas presented in literature[7,8]

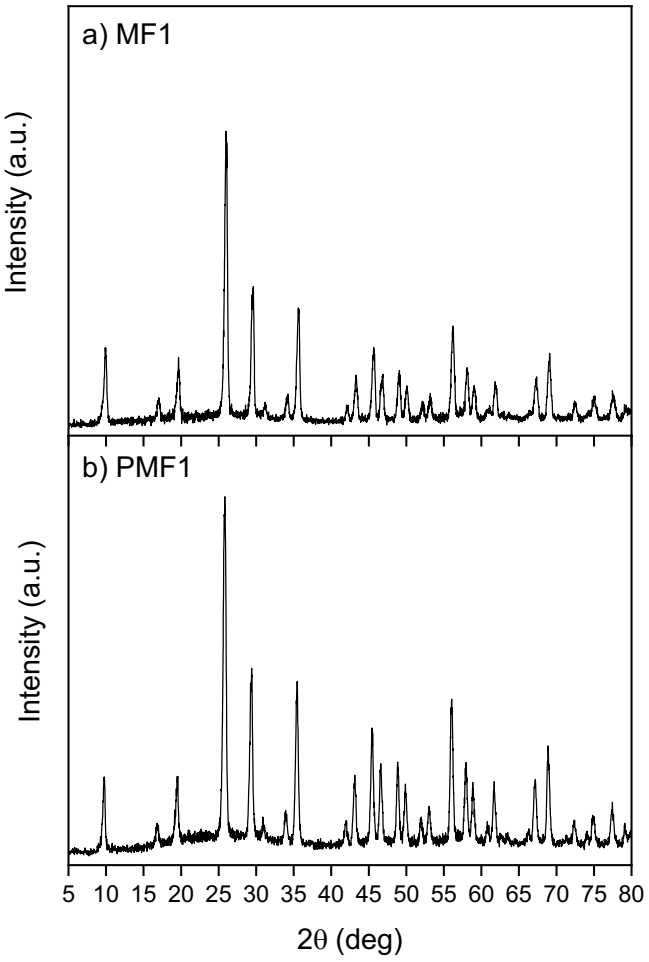

Figure S3: XRD Pattern of a) MF1 and b) PMF1

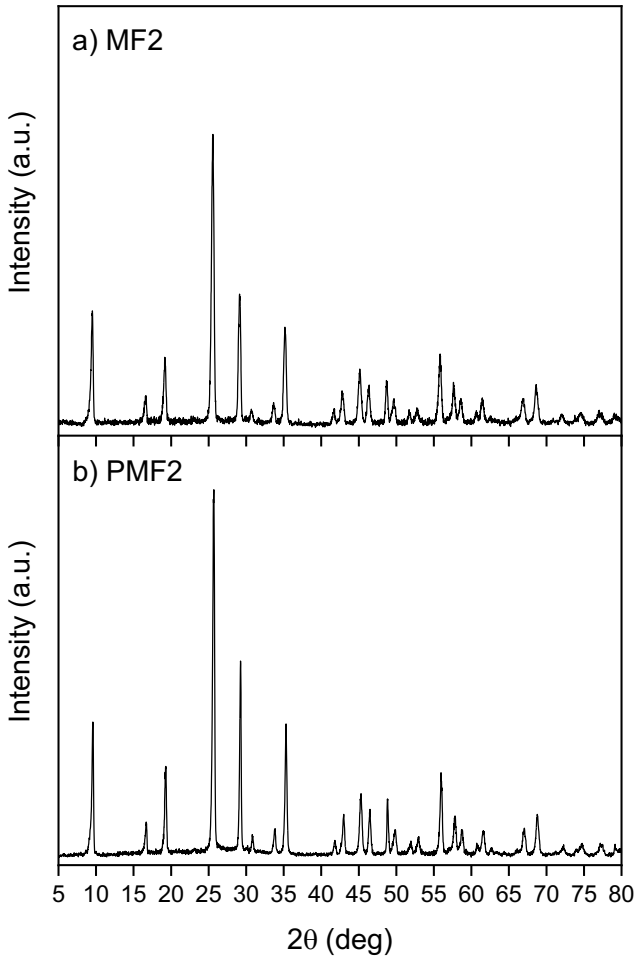

Figure S4: XRD Pattern of a) MF2 and b) PMF2

Table S5. Relative atomic concentrations from XPS

Material	C (%)	O (%)	Mo (%)	Fe (%)	Other (%)
MF1	13.6	60.8	25.3	0.3	
PMF1	31.3	47.8	16.7	0.4	N: 2.8, S: 1.0
MF2	19.1	57.8	21.8	1.3	
PMF2	51.2	33.9	12.8	0.1	N: 1.3, Cl: 0.7

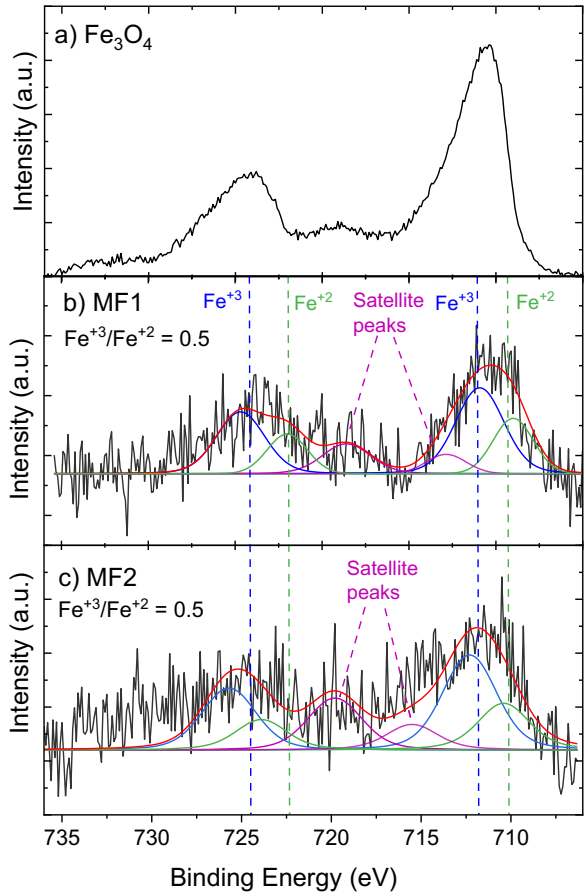

Figure S5. XPS Fe 2p spectra of a) Fe_3O_4 and the fitted spectra of b) MF1 and c) MF2

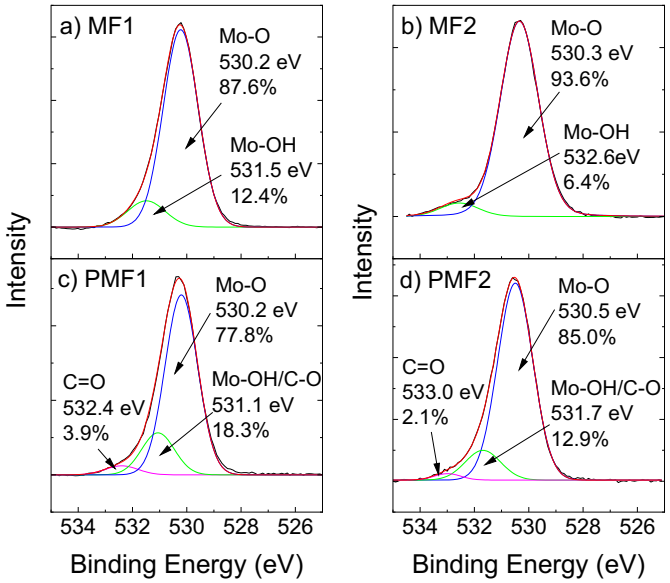

Figure S6. XPS O1s fitted spectra

Table S6. Molybdenum XPS fitting parameters

Material	Peak type	Peak Center (eV)	FWHM (eV)	Area	Concentration %
MF1	Mo $3d_{5/2}$ (Mo^{+6})	232.57	1.31	49196.01	56.0
	Mo $3d_{3/2}$ (Mo^{+6})	235.72	1.31	31942.06	36.3
	Mo $3d_{5/2}$ (Mo^{+5})	231.45	1.21	4053.00	4.6
	Mo $3d_{3/2}$ (Mo^{+5})	234.60	1.21	2701.69	3.1
MF2	Mo $3d_{5/2}$ (Mo^{+6})	232.59	1.37	37399.71	57.3
	Mo $3d_{3/2}$ (Mo^{+6})	235.77	1.37	24889.87	38.1
	Mo $3d_{5/2}$ (Mo^{+5})	231.51	1.27	1774.23	2.7
	Mo $3d_{3/2}$ (Mo^{+5})	234.66	1.27	1227.52	1.9

Table S7. ATR-FTIR peaks and corresponding bond vibrations of Fe_3O_4, MoO_3, MF1, PMF1, MF2, and PMF2

Fe_3O_4	MoO_3	PPy	PANI	MF1	PMF1	MF2	PMF2	Functional group/assignment
-	-		1564.7 cm^{-1}	-	-	-	1606.9 cm^{-1}	C=C-C stretching vibrations (PANI-quinoid diamine, N=Q=N)[9–12]
-	-	1552.4 cm^{-1}	-	-	1552.0 cm^{-1}	-	-	Pyrrole ring vibrations(C=C stretching)[11–14]
-	-	-	1488.3 cm^{-1}	-	-	-	-	C=C-C aromatic ring stretching of the benzenoid diamine (N-B-N)[9,10,14]
-	-	1461.8 cm^{-1}	-	1433.4 cm^{-1}	1443.5 cm^{-1}	1442.5 cm^{-1}	1442.0 cm^{-1}	C-N stretching[10,11,13,15]
-	1403.5 cm^{-1}	-	-	1405.2 cm^{-1}	-	1405.7 cm^{-1}	-	N-H bending[16,17]
-	-	1305.1 cm^{-1}	-	-	1317.6 cm^{-1}	-	-	C-H in-plane vibrations[9,15]
-	-	-	1296.0 cm^{-1}	-	-	-	1305.6 cm^{-1}	C-N stretching [10,18]
-	-	-	1245.0 cm^{-1}	-	-	-	1246.8 cm^{-1}	$C-N^+$ stretching[19,20]
-	-	1174.5 cm^{-1}	-	-	-	-	-	C-N stretching[11,12]
-	-	1042.8 cm^{-1}	~1145-~1038 cm^{-1}	-	-	-	-	C-H in plane vibrations[9,13,15,19,20]
-	956.1 cm^{-1}	-	-	969.6 cm^{-1}	965.2 cm^{-1}	972.4 cm^{-1}	971.5 cm^{-1}	M=O stretching[17,21]
-	895.3 cm^{-1}	-	-	895.8 cm^{-1}	896.8 cm^{-1}	895.8 cm^{-1}	895.3 cm^{-1}	M=O stretching[17,21]
-	878.9 cm^{-1}	-	-	-	-	-	-	M=O stretching[17,21]
-	-	-	797.5 cm^{-1}	-	-	-	-	C-H out of plane bending in aromatic ring[9,19,20]
-	568.4 cm^{-1}	-	-	579.5 cm^{-1}	579.0 cm^{-1}	571.8 cm^{-1}	565.1 cm^{-1}	Mo-O-Mo bending[10,16,17,21]
559.9 cm^{-1}	-	-	-	-	-	-	-	Fe-O-Fe bending[22]
-	517.3 cm^{-1}	-	-	517.4 cm^{-1}	518.3 cm^{-1}	517.8 cm^{-1}	517.3 cm^{-1}	Mo-O-Mo bending[21]

Table S8. Fitting curve values corresponding to equation 2 once polymerization was completed[a]

Material	Level[b]	G	R_g (Å)	B	P	Background (cm^{-1})	Reduced χ^2
PPy on MF1	1	23.9 ± 0.64	286.7 ± 0.95	4.72e-8 ± 1.62e-11	3.78 ± 1.52e-4	0.066 ± 7.26e-6	1.05
	2	312.4 ± 18.66	561.4 ± 5.56	8.23e-6 ± 3.40e-8	2.86 ± 0.007		
	3	3.35e5 ± 1.69e3	2744 ± 4.05	4.49e-7 ± 9.77e-11	3.61 ± 5.30e-4		
PPy on MF2	1	12.01 ± 0.57	259.9.00 ± 0.57	1.17e-7 ± 6.35e-11	3.53 ± 1.52e-4	0.064 ± 3.41e-6	1.14
	2	502.6 ± 4.93	635.4 ± 2.23	1.96e-5 ± 4.07e-8	2.73 ± 0.060		
	3	5.16e5 ± 1.10e4	3300 ± 5.97	4.36e-8 ± 1.39e-11	3.90 ± 1.54e-4		
PANI on MF1	1	1.37 ± 0.069	378.5 ± 110.46	3.19e-8 ± 1.66e-10	3.19 ± 9.63e-3	0.264 ± 1.41e-5	0.61
	2	50.71 ± 5.44	1245 ± 35.94	3.00e-5 ± 3.74e-7	2.03 ± 3.68e-3		
	3	1781 ± 2.75e3	2965.3 ± 236.72	1.06e-7 ± 2.31e-9	3.04 ± 7.88e-3		
PANI on MF2	1	1.87 ± 0.05	304.5 ± 4.43	8.07e-8 ± 3.26e-10	3.11 ± 0.005	0.20 ± 1.34e-5	1.06
	2	370.44 ± 8.18	1369 ± 9.15	1.70e-6 ± 1.11e-8	2.74 ± 0.001		
	3	3433.0 ± 1.63e3	2890 ± 21.03	1.47e-7 ± 5.11e-9	3.1 ± 0.007		
	4	0	1e10	1.71e-5 ± 1.23e-7	3.15 ± 0.083		

[a] G is a pre-factor for the Guinier exponential term, B is a pre-factor for the power law term, R_g is the radius of gyration of the structure feature, P describes the fractal dimension of the material, and the background arises from the incoherent scattering background of the samples. The reduced χ^2 value describes the goodness of fit where the closer the value is to 1 the better the fit;
[b] On each material, the Level 2 structure arose from the polymer.

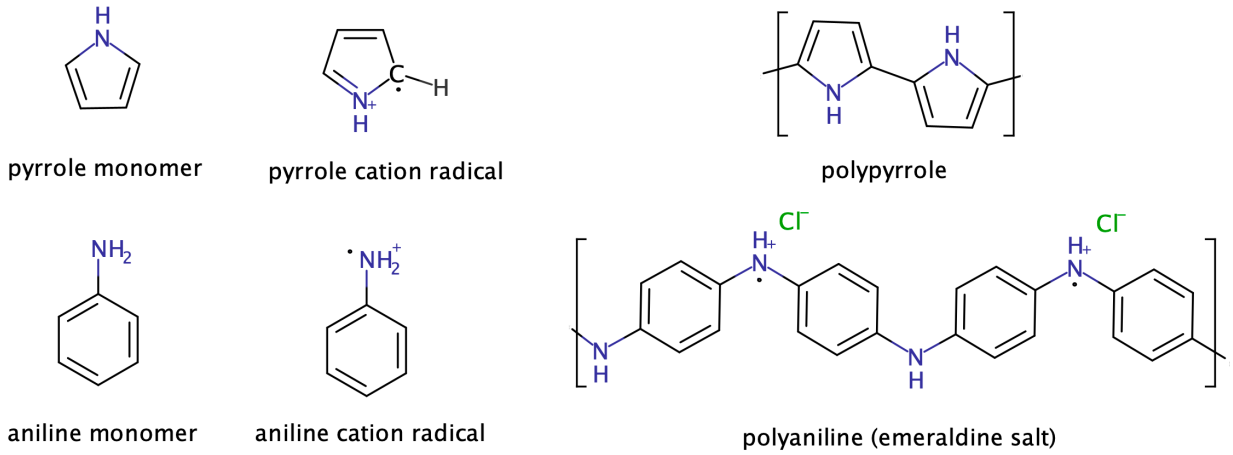

Scheme S1. Pyrrole and aniline monomers, cation radicals, and polymers

References

(1) Behera, S. K.; Meena, H.; Charaborty, S.; Meikap, B. C. Application of Response Surface Methodology (RSM) for Optimization of Leaching Parameters for Ash Reduction from Low-Grade Coal. *Int. J. Min. Sci. Technol.* **2018**, *28* (4), 621–629. https://doi.org/10.1016/j.ijmst.2018.04.014.

(2) Hu, Z.; Zhou, J.; Zhang, Y.; Liu, W.; Zhou, J.; Cai, W. The Formation of a Direct Z-Scheme Bi_2O_3/MoO_3 Composite Nanocatalyst with Improved Photocatalytic Activity under Visible Light. *Chem. Phys. Lett.* **2018**, *706*, 208–214. https://doi.org/10.1016/j.cplett.2018.06.006.

(3) Shafi, P. M.; Dhanabal, R.; Chithambararaj, A.; Velmathi, S.; Bose, A. C. α-MnO_2/h-MoO_3 Hybrid Material for High Performance Supercapacitor Electrode and Photocatalyst. *ACS Sustain. Chem. Eng.* **2017**, *5* (6), 4757–4770. https://doi.org/10.1021/acssuschemeng.7b00143.

(4) Rafaie, H. A.; Nor, R. M.; Azmina, M. S.; Ramli, N. I. T.; Mohamed, R. Decoration of ZnO Microstructures with Ag Nanoparticles Enhanced the Catalytic Photodegradation of Methylene Blue Dye. *J. Environ. Chem. Eng.* **2017**, *5* (4), 3963–3972. https://doi.org/10.1016/j.jece.2017.07.070.

(5) Yunarti, R. T.; Safitri, T. N.; Dimonti, L. C. C.; Aulia, G.; Khalil, M.; Ridwan, M. Facile Synthesis of Composite between Titania Nanoparticles with Highly Exposed (001) Facet and Coconut Shell-Derived Graphene Oxide for Photodegradation of Methylene Blue. *J. Phys. Chem. Solids* **2022**, *160* (August 2021), 110357. https://doi.org/10.1016/j.jpcs.2021.110357.

(6) Yang, H.; Li, X.; Wang, A.; Wang, Y.; Chen, Y. Photocatalytic Degradation of Methylene Blue by MoO_3 Modified TiO_2 under Visible Light. *Cuihua Xuebao/Chinese J. Catal.* **2014**, *35* (1), 140–147. https://doi.org/10.1016/S1872-2067(12)60731-1.

(7) Kamoun, O.; Mami, A.; Amara, M. A.; Vidu, R.; Amlouk, M. Nanostructured Fe,Co-Codoped MoO_3 Thin Films. *Micromachines* **2019**, *10* (2). https://doi.org/10.3390/mi10020138.

(8) Sundeep, D.; Gopala Krishna, A.; Ravikumar, R. V. S. S. N.; Vijaya Kumar, T.; Daniel Ephraim, S.; Pavan, Y. L. Spectral Characterization of Mechanically Synthesized MoO_3-CuO Nanocomposite. *Int. Nano Lett.* **2016**, *6* (2), 119–128. https://doi.org/10.1007/s40089-015-0178-z.

(9) Das, A. K.; Karan, S. K.; Khatua, B. B. High Energy Density Ternary Composite Electrode Material Based on Polyaniline (PANI), Molybdenum Trioxide (MoO_3) and Graphene Nanoplatelets (GNP) Prepared by Sono-Chemical Method and Their Synergistic Contributions in Superior Supercapacitive Performance. *Electrochim. Acta* **2015**, *180*, 1–15. https://doi.org/10.1016/j.electacta.2015.08.029.

(10) Bai, S.; Zhao, Y.; Sun, J.; Tong, Z.; Luo, R.; Li, D.; Chen, A. Preparation of Conducting Films Based on α-MoO_3/PANI Hybrids and Their Sensing Properties to Triethylamine at Room Temperature. *Sensors Actuators, B Chem.* **2017**, *239*, 131–138. https://doi.org/10.1016/j.snb.2016.07.174.

(11) Balakumar, V.; Kim, H. H.; Manivannan, R.; Kim, H. H.; Ryu, J. W.; Heo, G.; Son, Y. A. Ultrasound-Assisted Method to Improve the Structure of CeO_2@polyprrole Core-Shell Nanosphere and Its Photocatalytic Reduction of Hazardous Cr^{6+}. *Ultrason. Sonochem.* **2019**, *59*, 104738. https://doi.org/10.1016/j.ultsonch.2019.104738.

(12) Sahoo, N. G.; Jung, Y. C.; So, H. H.; Cho, J. W. Polypyrrole Coated Carbon Nanotubes: Synthesis, Characterization, and Enhanced Electrical Properties. *Synth. Met.* **2007**, *157* (8–9), 374–379. https://doi.org/10.1016/j.synthmet.2007.04.006.

(13) Zhang, X.; Zeng, X.; Yang, M.; Qi, Y. Investigation of a Branchlike MoO_3/Polypyrrole Hybrid with Enhanced Electrochemical Performance Used as an Electrode in Supercapacitors. *ACS Appl. Mater. Interfaces* **2014**, *6* (2), 1125–1130. https://doi.org/10.1021/am404724u.

(14) Razalli, R. L.; Abdi, M. M.; Tahir, P. M.; Moradbak, A.; Sulaiman, Y.; Heng, L. Y. Polyaniline-Modified Nanocellulose Prepared from Semantan Bamboo by Chemical Polymerization: Preparation and Characterization. *RSC Adv.* **2017**, *7* (41), 25191–25198. https://doi.org/10.1039/c7ra03379f.

(15) Cetiner, S.; Karakas, H.; Ciobanu, R.; Olariu, M.; Kaya, N. U.; Unsal, C.; Kalaoglu, F.; Sarac, A. S. Polymerization of Pyrrole Derivatives on Polyacrylonitrile Matrix, FTIR-ATR and Dielectric Spectroscopic Characterization of Composite Thin Films. *Synth. Met.* **2010**, *160* (11–12), 1189–1196. https://doi.org/10.1016/j.synthmet.2010.03.007.

(16) Chithambararaj, A.; Sanjini, N. S.; Bose, A. C.; Velmathi, S. Flower-like Hierarchical h-MoO_3: New Findings of Efficient Visible Light Driven Nano Photocatalyst for Methylene Blue Degradation. *Catal. Sci. Technol.* **2013**, *3* (5), 1405–1414. https://doi.org/10.1039/c3cy20764a.

(17) Wongkrua, P.; Thongtem, T.; Thongtem, S. Synthesis of h- and α-MoO_3 by Refluxing and Calcination Combination: Phase and Morphology Transformation, Photocatalysis, and Photosensitization. *J. Nanomater.* **2013**, *2013*. https://doi.org/10.1155/2013/702679.

(18) Anilkumar, K. R.; Parveen, A.; Badiger, G. R.; Ambika Prasad, M. V. N. Effect of Molybdenum Trioxide (MoO_3) on the Electrical Conductivity of Polyaniline. *Phys. B Condens. Matter* **2009**, *404* (12–13), 1664–1667. https://doi.org/10.1016/j.physb.2009.01.046.

(19) Shao, W.; Jamal, R.; Xu, F.; Ubul, A.; Abdiryim, T. The Effect of a Small Amount of Water on the Structure and Electrochemical Properties of Solid-State Synthesized Polyaniline. *Materials (Basel).* **2012**, *5* (10), 1811–1825. https://doi.org/10.3390/ma5101811.

(20) Lissarrague, M. H.; Lamanna, M. E.; D'Accorso, N. B.; Goyanes, S. Effects of Different Nucleating Particles on Aniline Polymerization. *Synth. Met.* **2012**, *162* (11–12), 1052–1058. https://doi.org/10.1016/j.synthmet.2011.12.018.

(21) Peña-Bahamonde, J.; Wu, C.; Fanourakis, S. K.; Louie, S. M.; Bao, J.; Rodrigues, D. F. Oxidation State of Mo Affects Dissolution and Visible-Light Photocatalytic Activity of MoO_3 Nanostructures. *J. Catal.* **2020**, *381*, 508–519. https://doi.org/10.1016/j.jcat.2019.11.035.
(22) Yusoff, A. H. M.; Salimi, M. N.; Jamlos, M. F. Synthesis and Characterization of Biocompatible Fe_3O_4 Nanoparticles at Different PH. *AIP Conf. Proc.* **2017**, *1835* (April 2017), 1–5. https://doi.org/10.1063/1.4981832.